



This is a repository copy of *Online thermal parameter identification for permanent magnet synchronous machines*.

White Rose Research Online URL for this paper:  
<http://eprints.whiterose.ac.uk/164680/>

Version: Accepted Version

---

**Article:**

Xiao, S. and Griffo, A. (2020) Online thermal parameter identification for permanent magnet synchronous machines. IET Power Electronics, 14 (12). pp. 2340-2347. ISSN 1751-8660

<https://doi.org/10.1049/iet-epa.2020.0119>

---

This paper is a postprint of a paper submitted to and accepted for publication in IET Electric Power Applications and is subject to Institution of Engineering and Technology Copyright. The copy of record is available at the IET Digital Library

**Reuse**

Items deposited in White Rose Research Online are protected by copyright, with all rights reserved unless indicated otherwise. They may be downloaded and/or printed for private study, or other acts as permitted by national copyright laws. The publisher or other rights holders may allow further reproduction and re-use of the full text version. This is indicated by the licence information on the White Rose Research Online record for the item.

**Takedown**

If you consider content in White Rose Research Online to be in breach of UK law, please notify us by emailing [eprints@whiterose.ac.uk](mailto:eprints@whiterose.ac.uk) including the URL of the record and the reason for the withdrawal request.



[eprints@whiterose.ac.uk](mailto:eprints@whiterose.ac.uk)  
<https://eprints.whiterose.ac.uk/>

# Online Thermal Parameter Identification for Permanent Magnet Synchronous Machines

Shuai Xiao<sup>1\*</sup>, Antonio Griffio<sup>2</sup>

<sup>1</sup>Department of Electronic and Electrical Engineering, The University of Sheffield, 3 Solly Street, Sheffield, U.K.

<sup>2</sup>Department of Electronic and Electrical Engineering, The University of Sheffield, F125 Mappin Building, Sheffield, U.K.

\*[mxiao0601@gmail.com](mailto:mxiao0601@gmail.com)

**Abstract:** Temperature monitoring of permanent magnet synchronous machines (PMSMs) is of great importance because high temperatures can significantly shorten the lifetimes of motor components. Accurate temperature predictions can be achieved using reduced-order lumped parameter thermal networks (LPTN) with accurate thermal parameters. In this paper, an online estimation method based on the recursive Kalman Filter algorithm is introduced for online identification of the thermal resistances in a three-node LPTN representing motor stator iron, stator winding and permanent magnet. The identification procedure requires a rotor temperature measurement, which is provided by an accurate PWM-based estimation method. The proposed methodology is experimentally validated and applied to real-time fault detection of the motor cooling system.

## 1. Introduction

The use of electric machines can be found in many applications such as household appliance, machine tools, vehicles and railways, due to their indispensable role in converting energy. Permanent magnet synchronous machines (PMSMs) most recently have been increasingly employed in electrical/hybrid electrical vehicles, industrial servo drives and wind power generators for their high-power density and good efficiency. There is a growing trend towards the inclusion of the thermal management in permanent magnet synchronous machines by monitoring their internal temperatures during real-time operation, because high temperature is one of the main stressors causing motor state-of-health degradation and ultimately failure [1]. With regard to the motor stator, temperature limit normally occurs in stator winding insulation, which is classified according to maximum allowable stator winding operating temperature. Thermal overload can significantly shorten the lifetime of stator insulation [2]. Excessive thermal stress also increases the risk of partial, or even irreversible demagnetization of rotor magnet [3], [4], especially with motor operating in flux weakening mode. Therefore, thermal monitoring of PMSMs is particularly significant.

Several direct and indirect motor temperature monitoring techniques are well established. Temperature sensors are suitable for stator temperature measurement, as they can be relatively easily fixed into motor stators during manufacturing process. Nevertheless, the use of temperature sensors may require additional costs and increase system complexity. Rotor temperature measurement is particularly difficult in practice, because only slip rings [5], [6], infrared [7], [8] and wireless sensors [9], [10] can access the rotating parts of a motor. Besides, extra instruments are required for the processing and transmission of temperature data, and they are limited to laboratory use [11]. Hence model-based methods have been at the centre of research interest in recent years.

Motor temperatures can be derived from temperature-dependent electrical parameters. Stator winding temperatures can be predicted based on its linear relationship with stator resistance. In [12], a DC voltage offset is injected intermittently into one or more motor phases. As a result, winding resistance estimation is dependent on the variations in rotor flux linkage and inductances. However, the injection of DC voltage creates disturbances to the operation of the motor. Alternatively, ref. [13] introduces a new estimation scheme involving the use of the recursive least square (RLS) algorithm. The value of stator resistance therefore can be updated continuously in real-time. It is also possible to determine rotor temperature via the thermal property of PM flux linkage, as (NdFeB) magnet loses approximately 0.1% remanence for one-degree Celsius rotor temperature rise [14]. An online method estimating PM flux linkage and stator resistance using a full-rank motor model corresponding to  $i_d = 0$  and an injected  $i_d \neq 0$  test signal is introduced in [15]. Nonetheless, signal injection produces undesired ripples and losses disturbing motor operation. The use of rotor flux linkage observer is presented in [3], [16], in which the variation in flux linkage due to rotor temperature change is retrieved from the difference in stator current. As many other methods of the similar type, it requires accurate modelling for motor and inverter in order to avoid the model-related errors being misinterpreted as rotor temperature variations.

Another commonly employed approach is based upon the use of a lumped parameters thermal network (LPTN). It informs a ‘thermal estimator’, which after being integrated with a robust loss model, can provide accurately estimated motor temperatures during real-time operation. Several thermal models with high complexity for induction motors (IMs) and PMSMs are proposed in [17]-[19]. They are designed to estimate the temperatures at multiple locations in the machine. Nevertheless, they are modelled mainly based on the motor geometry and material information, which may not be directly accessible in practice. Furthermore, an accurate prediction of motor losses and the derivations of heat transfer coefficients can be complicated and empirical

formulas may need to be used. One such high-fidelity and computationally efficient model for interior PMSMs (IPMSMs) is presented in [20], in which the power losses are computed by an electromagnetic motor model considering saturation, harmonics, iron loss and temperature effects, and then passed on to a 48-node thermal network derived from the Finite Element (FE) software for the temperature estimations. A low-order LPTN summarizes the major heat paths in a motor and the identification of the thermal parameters can be performed based on the minimization of the difference between the experimental training data and estimation — detailed knowledge regarding the motor dimensions and materials therefore may not be required [2], [4], [21], [22]. Although several, experimentally based, methods for parameters identification of a LPTN have been proposed [4], most are based on offline procedures during drive commissioning. In practice, many parameters are often unknown or difficult to estimate, e.g. in interfaces between materials, mechanical mounting, environmental conditions, cooling system etc. adding significant uncertainties to the parameter estimation task. Additionally, thermal parameters might change during motor operation due e.g. to deterioration of the cooling conditions, faults in cooling fans, obstructions of coolant flow, build-up of contaminants, dust, etc [23]. These phenomena cannot be modelled by a LPTN whose parameters are constant and extracted during commissioning. Therefore, an identification process with a continuous online update mechanism for the parameters might be beneficial for the thermal monitoring of motors. An additional potential application would be the detection of impaired cooling conditions [23].

This paper proposes a practical and computationally efficient method for online identification of the thermal parameters in a reduced-order LPTN which represents stator iron, stator winding and permanent magnet. The thermal structure can be described by a set of state-space equations in which the losses are derived from motor electrical parameters, such as stator current and rotor speed, whereas the thermal capacitances are obtained via FE thermal analysis. A recursive parameter identification procedure is employed for the calculation of the thermal resistances, which requires an accurate rotor temperature measurement. This is provided by a PWM-based estimation method predicting rotor temperature via motor PM flux linkage [24], instead of by temperature sensors which are expensive and difficult to implement in practice. Due to the inclusion of the heat path between stator and cooling in the thermal network, the proposed method can potentially be able to detect the errors and sudden changes to motor cooling system, which will be reflected on the variation in the corresponding thermal resistance identified in real-time. The presented method could be implemented for PMSMs with different topologies and sizes. In this paper, comprehensive experimental validations of the methodology are conducted on a three-phase surface-mounted PM servo motor (SPMSM) in a board range of motor operations and at two different cooling conditions.

The main contributions of this paper include:

- An online method, as opposed to the more common offline methods, for the identification of parameters of the thermal model of a PMSM.

- An application of the method to the detection of faulty conditions in cooling system is also demonstrated.
- The integration of the thermal model and a PWM-based rotor temperature estimation method [24] which provides an accurate measurement for the parameter identification and cross-validation.

## 2. Fundamental Theory

### 2.1. Model Structure

A reduced-order LPTN with three temperature nodes and considering only the most significant heat transfer processes in the motors is introduced for real-time temperature estimation for PMSM.

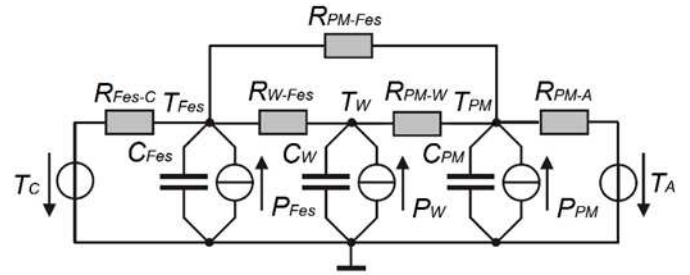


Fig. 1. Schematic graph of the three-node LPTN [25]

As illustrated in Fig. 1, the nodes correspond to stator iron ( $T_{Fes}$ ), stator winding ( $T_W$ ), and rotor permanent magnets ( $T_{PM}$ ). The thermal resistance between stator iron and stator winding  $R_{W-Fes}$  represents the heat conduction through the solid regions of a motor. The heat convection through air gap is described by  $R_{PM-Fes}$  and  $R_{PM-W}$ , whereas the heat flows to cooling system and ambient, which are represented by two temperature sources  $T_C$  and  $T_A$ , respectively, are depicted as  $R_{Fes-C}$  and  $R_{PM-A}$ . Each node is also connected to a heat source  $P$  being the heat losses of the respective region of the motor, as well as a thermal capacitance  $C$ , which is the product of the specific heat capacity and the mass of the respective motor component and therefore is assumed to be constant.

It is important that the thermal resistance  $R_{PM-A}$  is taken into account. Physically it represents the heatflow from rotor to ambient through the motor shaft. The rotor temperature otherwise may be overestimated in cases where both the stator iron and stator winding temperatures are higher than the rotor temperature, because there is no power outlet for the PM node.

### 2.2. Loss Modelling

An accurate modelling of motor losses is of the essence because it describes the heat generation in a motor and thus affects the thermal behavior of the motor. The losses are calculated based on motor speeds and electric currents, which are commonly available in the motor controller. The three-phase copper loss generated by the active winding and end-winding of a motor can be expressed as:

$$P_W = 3I_{rms}^2 R_s(T_W) \quad (1)$$

The stator resistance  $R_s$  is assumed to be linearly dependent on the winding temperature  $T_W$  as:

$$R_s(T_W) = R_{s0}[1 + \alpha_{cu}(T_W - T_0)] \quad (2)$$

where  $R_{s0}$  is the phase resistance at room temperature  $T_0$ , and  $\alpha_{cu}$  is a temperature coefficient for copper  $\alpha_{cu} = 0.393\%/^\circ\text{C}$ .  $T_W$  is the average winding temperature which can be obtained from temperature sensors. The rms current in (1) should account for the fundamental and any higher order harmonics current, if present.

The on-load iron loss is assumed to be the superposition of the two modes of motor operations corresponding to two distinct flux paths — the main magnetizing flux path associated with the PM and stator current, and the field weakening path relating to the demagnetizing current [25]. The iron loss models presented in [26] are adopted, which after taking into consideration the dependence of the flux linkage on the magnet temperature  $T_{PM}$ , can be described as:

$$P_{OC} = a_h f \left( \frac{\sqrt{\psi_d^2(T_{PM}) + \psi_q^2(T_{PM})}}{\psi_m(T_0)} \right) + a_e f^2 \left( \frac{\sqrt{\psi_d^2(T_{PM}) + \psi_q^2(T_{PM})}}{\psi_m(T_0)} \right)^2 \quad (3)$$

$$P_{SC} = b_h f \left( \frac{|\psi_d(T_{PM}) - \psi_m(T_{PM})|}{\psi_m(T_0)} \right) + b_e f^2 \left( \frac{|\psi_d(T_{PM}) - \psi_m(T_{PM})|}{\psi_m(T_0)} \right)^2 \quad (4)$$

where  $f$  is the electrical frequency at which the iron loss is calculated. The iron losses in (3) and (4) are split into the hysteresis and eddy current components. The constants ( $a_h$ ,  $a_e$ ) and ( $b_h$ ,  $b_e$ ) can be calculated by the finite element analysis at open-circuit and short-circuit operations, respectively, and room temperature  $T_0$ . These parameters are summarized in Table 1. The total iron loss at a given operating condition is the sum of the loss in relation to the main magnetizing flux path  $P_{OC}$  and field-weakening induced loss  $P_{SC}$ . In this application, the motor is not controlled in field-weakening region, which means  $P_{SC} = 0$ .  $\psi_d$  and  $\psi_q$  are the  $dq$ -axis flux linkages, which considering the demagnetizing field  $\psi_d^*$  can be written as:

$$\psi_d = L_d i_d + \psi_m + \psi_d^* \quad (5)$$

$$\psi_q = L_q i_q \quad (6)$$

where  $\psi_d^* = 0$  due to the tested motor operating only at the rated flux.

**Table 1** Parameters Calculated by FEA

Quantity	Unit	Value
$a_h$	W/Hz	0.0093
$a_e$	W/(Hz) <sup>2</sup>	$3.08 \times 10^{-5}$
$b_h$	W/Hz	0.0010
$b_e$	W/(Hz) <sup>2</sup>	$5.51 \times 10^{-6}$

In practice, motor inductances may vary due to saturation. For the motor used in the following,  $L_d$  and  $L_q$  are

not subject to this effect at the current level applied ( $< 5 \text{ A}$ ) and therefore are assumed to be constant in (5)-(6).

Rotor losses  $P_{PM}$  can also be included in the model. In this application, they are assumed to be negligible to simplify the modelling process due to the relatively low-speed operation of the tested motor.

### 2.3. Thermal Capacitance and Resistance

The thermal capacitance of a motor component is defined by its specific heat capacity and mass and can be calculated with the knowledge of the motor topology. The precise calculation of the thermal capacitance for each node in Fig. 1 is difficult because some uncertainties exist, for instance, the information regarding stator slot such as impregnation materials and insulation thickness is normally unknown.

The capacitances of the LPTN are calculated using the mass of the relative machine's part. Therefore, only the general knowledge of the machine geometry and material is required. Alternatively, FE thermal analysis, and/or commercial thermal analysis software e.g. MotorCAD, can be used. The capacitances  $C_{Fes}$ ,  $C_W$  and  $C_{PM}$  in Fig. 1 are estimated on the basis that the capacitance of each node is the sum of the capacitances of all the motor components this node represents. Specifically, the stator iron node capacitance consists of the stator housing, stator back iron, stator tooth, and flange mounted plate capacitances, etc. The winding node capacitance contains the stator winding and end-winding capacitances. Due to the lumped modelling of rotor, the PM node should be viewed as the 'rotor node' and therefore the capacitance of each component located in the rotor should be lumped together.

The proposed structure only takes into account the most important heat paths in a motor, which are summarized in five thermal resistances. These thermal resistances can be accurately determined using analytical formulas. However, due to the lack of detailed information concerning the motor internal topology, materials and interfaces etc., the thermal resistances are estimated in the parameter identification process introduced in the following section, along with the node temperatures.

### 2.4. Model Mathematical Expression and Discretization

The thermal behavior of the LPTN can be expressed in the form of a set of state-space equations:

$$\dot{\mathbf{x}} = \mathbf{A}\mathbf{x} + \mathbf{B}\mathbf{u} \quad (7)$$

$$\mathbf{y} = \mathbf{C}\mathbf{x} + \mathbf{D}\mathbf{u} \quad (8)$$

in which:

$$\mathbf{x} = [T_{Fes}, T_W, T_{PM}]^T \quad (9)$$

$$\mathbf{u} = [P_{Fes}, P_W, P_{PM}, T_C, T_A]^T \quad (10)$$

The state vector  $\mathbf{x}$  contains the node temperatures, whilst the input vector  $\mathbf{u}$  represents the power loss of each node and the motor cooling system and ambient temperatures  $T_C$  and  $T_A$ . The state and input matrices  $\mathbf{A}$  and  $\mathbf{B}$  are  $3 \times 3$  and  $3 \times 5$  vectors, respectively, and they are the functions of the thermal resistances and capacitances. With regard to  $\mathbf{C}$  and  $\mathbf{D}$ , they are identity and zero matrices, respectively, such that  $\mathbf{y}$  outputs the node temperatures.

For the purpose of real-time system identification, the discretization of the continuous model is required. The approach applied to discretizing the presented thermal model is the explicit Euler method (RK1), which does not require extensive numerical computations. The discrete-time model therefore is given as:

$$\mathbf{x}(k+1) = (T_k \mathbf{A}(k) + \mathbf{I})\mathbf{x}(k) + T_k \mathbf{B}(k)\mathbf{u}(k) \quad (11)$$

$$\mathbf{y}(k) = \mathbf{C}(k)\mathbf{x}(k) + \mathbf{D}(k)\mathbf{u}(k) \quad (12)$$

where  $k$  is the sampling index, and  $T_k$  is the sampling time set to a small value, such as 1 s, to avoid significant estimation errors.

## 2.5. Parameter Identification

The thermal resistances in the LPTN are estimated using a measurement-informed identification procedure, based on the recursive Kalman Filter algorithm, which can update continuously in real-time the values of the unknown state variables according to the minimization of the following cost function:

$$\min_x \sum_{k=1}^N \mathbf{e}_x(k)\mathbf{e}_x(k)^T \quad (13)$$

in which  $\mathbf{e}_x(k)$  is the state variables estimation error.

The identification problem can be formulated as a state observer with eight states. Three of the states correspond to the node temperatures of the thermal network. Five additional states represent the unknown thermal resistances in the network. The system has a nonlinear character due to the formulation where both temperatures and parameters are to be estimated. As a result, the extended Kalman Filter (EKF) which uses a continuously updated linearization is adopted to deal with the nonlinearity of the model. The state-space models of the nonlinear system can be described as:

$$\mathbf{x}_k = \mathbf{f}(\mathbf{x}_{k-1}, \mathbf{u}_k) + \mathbf{w}_k \quad (14)$$

$$\mathbf{z}_k = \mathbf{h}(\mathbf{x}_k) + \mathbf{v}_k \quad (15)$$

The process and measurement/observation noises  $\mathbf{w}_k$  and  $\mathbf{v}_k$  are assumed to be zero-mean white noises with covariances  $\mathbf{Q}_k$  and  $\mathbf{R}_k$  respectively. In this application, it is assumed that:

$$\mathbf{Q}_k = \mathbf{w}_k \mathbf{w}_k^T \quad (16)$$

$$\mathbf{R}_k = \mathbf{v}_k \mathbf{v}_k^T \quad (17)$$

where:

$$\mathbf{Q}_k = \begin{bmatrix} 0.0001 & 0 & 0 & 0 \\ 0 & 0.0001 & 0 & 0 \\ 0 & 0 & \ddots & \vdots \\ 0 & 0 & \dots & 0.0001 \end{bmatrix}^{8 \times 8} \quad (18)$$

$$\mathbf{R}_k = \begin{bmatrix} 0.01 & 0 & 0 & 0 \\ 0 & 0.01 & 0 & 0 \\ 0 & 0 & \ddots & \vdots \\ 0 & 0 & \dots & 0.01 \end{bmatrix}^{8 \times 8} \quad (19)$$

This combination ensures a strong weight being given to the measurements in the updating of the state estimates without them being overly noisy.

The algorithm performs a two-step process at each sampling time:

- Predict:

$$\hat{\mathbf{x}}_{k|k-1} = \mathbf{f}(\hat{\mathbf{x}}_{k-1|k-1}, \mathbf{u}_k) \quad (20)$$

$$\mathbf{P}_{k|k-1} = \mathbf{F}_k \mathbf{P}_{k-1|k-1} \mathbf{F}_k^T + \mathbf{Q}_k \quad (21)$$

- Update:

$$\hat{\mathbf{y}}_k = \mathbf{z}_k - \mathbf{h}(\hat{\mathbf{x}}_{k|k-1}) \quad (22)$$

$$\mathbf{S}_k = \mathbf{H}_k \mathbf{P}_{k|k-1} \mathbf{H}_k^T + \mathbf{R}_k \quad (23)$$

$$\mathbf{K}_k = \mathbf{P}_{k|k-1} \mathbf{H}_k^T \mathbf{S}_k^{-1} \quad (24)$$

$$\hat{\mathbf{x}}_{k|k} = \hat{\mathbf{x}}_{k|k-1} + \mathbf{K}_k \hat{\mathbf{y}}_k \quad (25)$$

$$\mathbf{P}_{k|k} = (\mathbf{I} - \mathbf{K}_k \mathbf{H}_k) \mathbf{P}_{k|k-1} \quad (26)$$

where:

$$\mathbf{F}_k = \frac{d\mathbf{f}}{d\mathbf{x}} \Big|_{\hat{\mathbf{x}}_{k-1|k-1}, \mathbf{u}_k} \quad (27)$$

$$\mathbf{H}_k = \frac{d\mathbf{h}}{d\mathbf{x}} \Big|_{\hat{\mathbf{x}}_{k|k-1}} \quad (28)$$

In the prediction step, the EKF computes the ‘a priori’ estimates  $\hat{\mathbf{x}}_{k|k-1}$  based on the state function  $\mathbf{f}$ , and the covariance matrix  $\mathbf{P}_{k|k-1}$ , using the state-transition Jacobian  $\mathbf{F}_k$  — a matrix of partial derivatives linearizing the system function. The update phase provides the ‘a posteriori’ estimates  $\hat{\mathbf{x}}_{k|k}$  by adding a corrective term  $\mathbf{K}_k \hat{\mathbf{y}}_k$  to the ‘a priori’ estimates in order to take into account the measurement information. The Kalman gain matrix  $\mathbf{K}_k$  is derived from the minimization of the trace of the updated covariance matrix  $\mathbf{P}_{k|k}$ .

However, it must be pointed out that, there may be more than one solution to the identification problem which guarantee the minimization of the squared error (13) due to the linearization step in the EKF.

## 2.6. Rotor Temperature Estimation

From the description above, it is clear that the identification of the thermal parameters requires temperature measurements, which can be acquired from temperature sensors. However, rotor temperature measurement remains a difficult task due to the challenge of placing sensors on a rotating shaft. An accurate estimation method which determines rotor temperature via PM flux linkage is a desirable solution to this issue.

In this paper, a relatively simple and accurate method is utilized for flux linkage and rotor temperature estimations, which only involves the use of the already-existing PWM voltage and stator current in response to the standard space-vector pulse width modulation (SV-PWM) [24]. The rotor flux linkage can be calculated by the  $q$ -axis voltage equation of a PMSM expressed as:

$$v_q = R_s i_q + L_q \frac{d}{dt} i_q + \omega_r (L_d i_d + \psi_m) \quad (29)$$

where  $v_q$ ,  $i_d$  and  $i_q$  are the  $q$ -axis voltage and  $dq$ -axis currents, respectively;  $L_d$ ,  $L_q$  and  $R_s$  are the  $dq$ -axis inductances and stator winding resistance.  $\omega_r$  is the rotor speed, and  $\psi_m$  denotes the rotor PM flux linkage.

The calculation takes place every single PWM switching period with the duration of  $t_{switching}$ , a simulation example of which is demonstrated in Fig. 2, where PWM1, PWM3 and PWM5 are the gate signals controlling the state of the three upper switches in a standard three-phase two-level voltage-fed inverter.  $t_1 \dots t_8$  are the time instants the active and zero-voltage vectors on the state vector diagram are applied.

Equation (29) is discretized adopting the RK1 method with a sampling time  $T_s \ll t_{switching}$ . Therefore, the derivative term can be written as:

$$di_q/dt \approx \frac{i_q(t_1+(k+1)T_s) - i_q(t_1+kT_s)}{T_s} \quad (30)$$

with  $k = 0, 1 \dots n - 1$ .  $n$  is the total number of sampling points in the period and the last point is  $t_8 = t_1 + (n - 1)T_s$ .

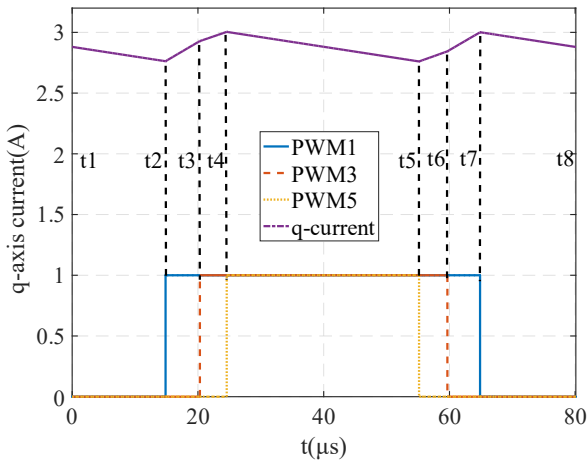


**Fig. 2.** Three-phase PWM signals and the corresponding  $q$ -current variation within one switching period [24]

Assuming the  $d$ -current to be controlled to zero, equation (29) becomes:

$$\begin{aligned} v_{q((t_1+kT_s)\sim(t_1+(k+1)T_s))} &= R_s i_{q((t_1+kT_s)\sim(t_1+(k+1)T_s))} \\ &+ L_q \frac{i_{q(t_1+(k+1)T_s)} - i_{q(t_1+kT_s)}}{T_s} \\ &+ \omega_r \psi_m \end{aligned} \quad (31)$$

With motor operating at steady-state, the current PI controller only regulates the  $q$ -current at the beginning of the non-zero-voltage switching periods (i.e.  $t_2$  and  $t_5$  in Fig. 2) and ensures that in steady-state they remain constant. This means that  $i_{q(t_2)} = i_{q(t_5)}$ ,  $i_{q(t_4)} = i_{q(t_7)}$  and  $i_{q(t_1)} = i_{q(t_8)}$ . Therefore, adding the  $n$  equations in the period gives:

$$T_s \sum v_{q(j)} = T_s R_s \sum i_{q(j)} + t_{switching} \omega_r \psi_m \quad (32)$$

where  $j$  is the  $j^{th}$  equation. It can be noticed that this expression is independent of  $L_q$ .

It is evident that the voltage sum  $T_s \sum v_{q(j)}$  in (32) is always identical to the average PWM output. In other words:

$$\begin{aligned} T_s \sum v_{q(j)} &= (t_3 - t_2) v_{q(t_3-t_2)} \\ &+ (t_4 - t_3) v_{q(t_4-t_3)} \\ &+ (t_6 - t_5) v_{q(t_6-t_5)} \\ &+ (t_7 - t_6) v_{q(t_7-t_6)} \end{aligned} \quad (33)$$

The following relations can be easily obtained considering that one SV-PWM switching period consists of two symmetrical pulse patterns:

$$(t_3 - t_2) v_{q(t_3-t_2)} = (t_7 - t_6) v_{q(t_7-t_6)} \quad (34)$$

$$(t_4 - t_3) v_{q(t_4-t_3)} = (t_6 - t_5) v_{q(t_6-t_5)} \quad (35)$$

Therefore, equation (33) now becomes:

$$\begin{aligned} 2[(t_3 - t_2) v_{q(t_3-t_2)} + (t_4 - t_3) v_{q(t_4-t_3)}] \\ = T_s R_s \sum i_{q(j)} \\ + t_{switching} \omega_r \psi_m \end{aligned} \quad (36)$$

The time intervals  $(t_3 - t_2)$  and  $(t_4 - t_3)$  are determined by the location of the reference voltage vector on the state vector diagram, and their corresponding  $q$ -axis voltage components  $v_{q(t_3-t_2)}$  and  $v_{q(t_4-t_3)}$  can be obtained by performing the  $\alpha\beta$ - $dq$  transformation on the two adjacent

active state vectors applied. In conclusion, the PM flux linkage can be calculated as:

$$\begin{aligned} \psi_m = \frac{f_{sw}}{\omega_r} 2[(t_3 - t_2) v_{q(t_3-t_2)} \\ + (t_4 - t_3) v_{q(t_4-t_3)}] \\ - \frac{f_{sw}}{\omega_r} T_s R_s \sum i_{q(j)} \end{aligned} \quad (37)$$

where  $f_{sw}$  is the PWM switching frequency and  $f_{sw} = 1/t_{switching}$ .

The  $q$ -axis current  $i_q$  is retrieved from the phase currents measurements using current sensors. The voltage reference is calculated from the phase voltages measured by voltage differential probes. The use of the command voltages generated by the controller should be avoided, because some inverter non-ideal effects, such as dead time, will significantly affect the accuracy of the estimation. The dependence of the stator resistance on the winding temperature is also taken into account by (2).

In addition, the noise in the current measurement may impact on the proposed method as a result of the approximation (30). Therefore, a low-pass filter with 1 Hz passband edge frequency is applied to the calculation (37) in order to obtain its average value. This is found adequate for the tracking of the flux linkage variations with rotor temperature, as the temperature changes comparatively slowly with typical time constants of many seconds/minutes.

It is assumed that flux linkage is linearly dependent on rotor temperature as:

$$\psi_m(T) = \psi_m(T_{ref}) [1 + \alpha_{\beta r} (T - T_{ref})] \quad (38)$$

in which  $\psi_m(T_{ref})$  is the flux linkage at the reference rotor temperature.  $\alpha_{\beta r}$  is a temperature-dependent coefficient and can be obtained from the open-circuit back-EMFs measured at two different rotor temperatures  $T_1$  and  $T_2$ :

$$\alpha_{\beta r} = \frac{1}{\psi_m(T_1)} \left[ \frac{\psi_m(T_2) - \psi_m(T_1)}{T_2 - T_1} \right] \quad (39)$$

Rotor temperature therefore can be derived from (38) and written as:

$$T = T_{ref} + \frac{1}{\alpha_{\beta r}} \left[ \frac{\psi_m(T)}{\psi_m(T_{ref})} - 1 \right] \quad (40)$$

### 3. Experimental Validation

#### 3.1. Experimental Setup

The validation of the proposed identification method is conducted on a two-motor dynamometer test rig built with a pair of three-phase PM servomotors (Teknic M-2310P-LN-04K). The rig is positioned in a metal enclosure and cooled by natural convection and radiation. The motor under test is connected to a three-phase MOSFET inverter and controlled with the Texas Instruments (TI) C2000 series FOC-enabled microcontroller LAUNCHXL-F28069M LaunchPad, whereas the second motor serves as a load and works as a generator connected to a three-phase resistive load. One K-type thermocouple is installed into the stator yoke to obtain the temperature measurement for the stator iron node. A second thermocouple is fitted inside the end-winding to acquire the winding node temperature. The rotor temperature measurement is calculated by the PWM-based rotor

temperature estimation method, which has been verified experimentally on the SPMSM employed also in this paper [24].

**Table 2** Parameters and Dimensions of the SPMSM

Quantity	Unit	Value
Continuous Torque	Nm	0.2754
Max Speed	r/min	6000
DC Link Voltage	V	24
Peak Current	A	7.1
No. of Pole-pairs	-	4
No. of Slots	-	18
Stator Resistance	Ohm	0.36
$d$ -axis Inductance	mH	0.1569
$q$ -axis Inductance	mH	0.1569
PM Flux Linkage	V/Hz	0.0409
Stator Outer Diameter	mm	51
Rotor Outer Diameter	mm	29

The parameter identification procedure is implemented on the FPGA-based real-time platform OPAL-RT 5600. A sampling time of  $10 \mu\text{s}$  is adopted for the calculation of the rotor temperature, in order to ensure that the total number of sampling points (10 points) and hence the total number of the voltage equations, in a PWM switching period ( $100 \mu\text{s}$ ) is integer. The computation of the thermal resistances takes place every minute, because the temperature variation is rather slow for the tested motor. However, it can be reduced to commonly used  $1 \text{ s}$ . The temperature measurements obtained from the thermocouples are converted into voltage signals by two temperature amplifiers powered by  $10 \text{ V}$  DC voltage, before being transferred into OPAL-RT where the conversion from voltage to temperature is performed.

### 3.2. Thermal Parameter Identification

The presented method is experimentally tested at a single-speed-single-current condition, where the identification of the unknown thermal resistances of the motor is carried out for more than three hours, until after the thermal equilibrium is reached. The results obtained in a wide range of motor speeds and currents ( $I_{mag} = \sqrt{i_d^2 + i_q^2}$ ) are demonstrated in Figs. 3-7. It is worth noting that the rotor temperature measurement predicted by the PWM-based method is less accurate at low speed due to the inherent difficulties of estimating the back-EMF [27].

Despite the fact that the cooling of the motor is through natural convection with ambient, which has a constant temperature, the resistances  $R_{Fes-C}$  and  $R_{PM-A}$  show dependence on motor operating conditions. This is because the natural convection coefficient  $h_1$ , and thus  $R_{Fes-C}$  and  $R_{PM-A}$  are dependent on the motor temperature, expressed as:

$$R_{natural} = \frac{1}{h_1 A_h} \quad (41)$$

$$h_1 = \frac{Nu_1 \lambda_{air}}{d_h} \quad (42)$$

$$Nu_1 = a(GrPr)^b \propto \Delta T_{motor-air} \quad (43)$$

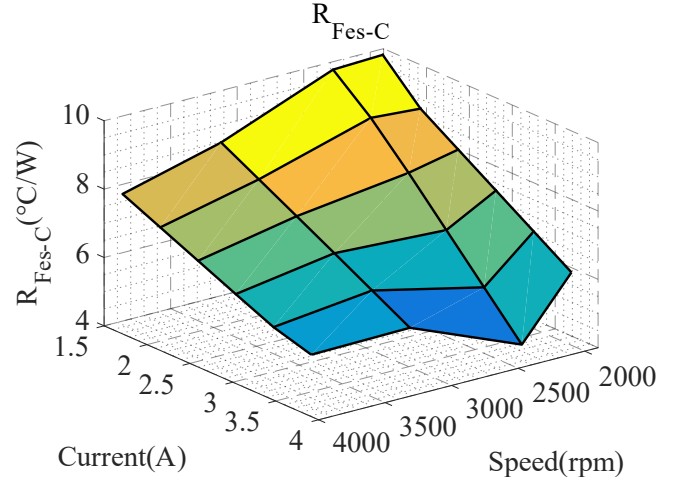


**Fig. 3.** Estimated thermal resistance  $R_{Fes-C}$  at different rotor speeds and stator currents

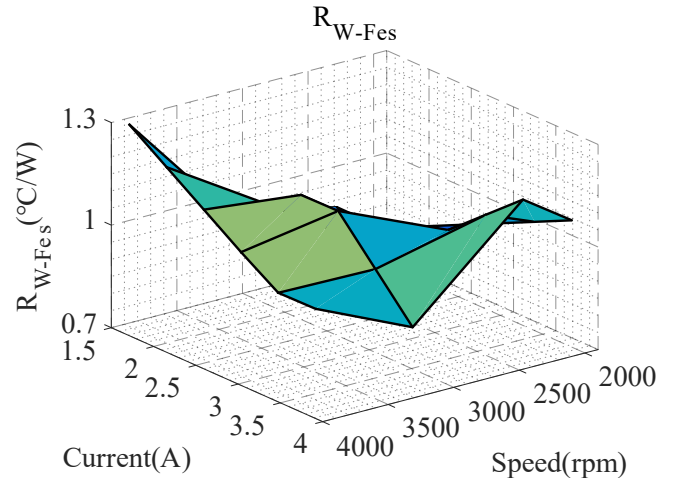


**Fig. 4.** Estimated thermal resistance  $R_{W-Fes}$  at different rotor speeds and stator currents

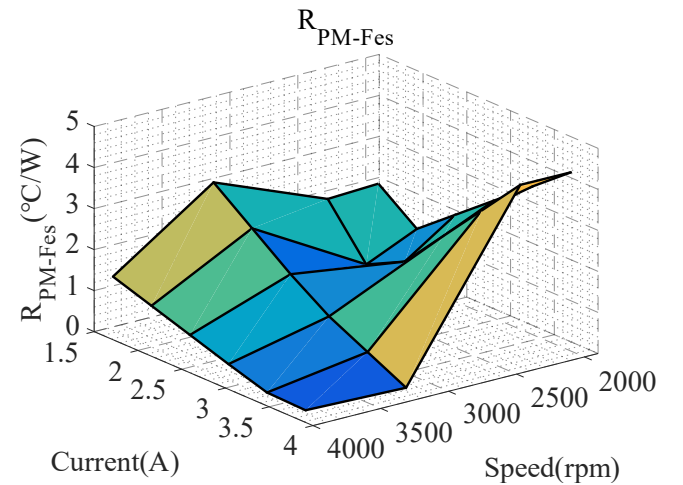


**Fig. 5.** Estimated thermal resistance  $R_{PM-Fes}$  at different rotor speeds and stator currents

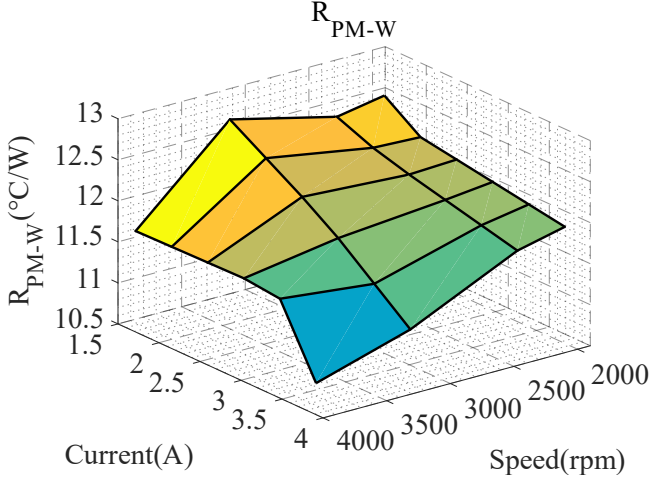


**Fig. 6.** Estimated thermal resistance  $R_{PM-W}$  at different rotor speeds and stator currents

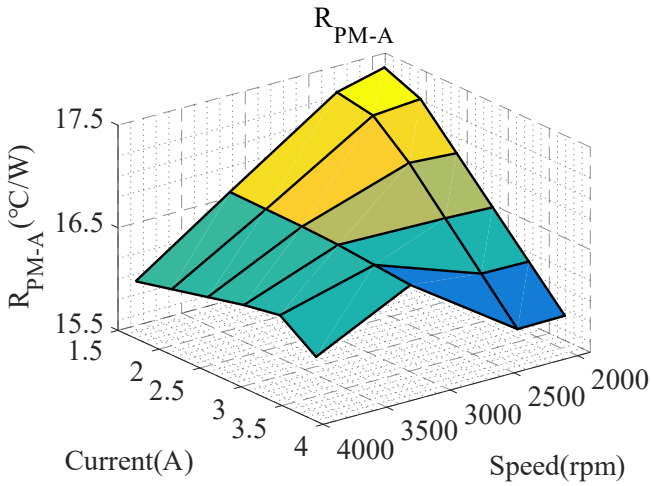


**Fig. 7.** Estimated thermal resistance  $R_{PM-A}$  at different rotor speeds and stator currents

where  $a$  and  $b$  are constants.  $A_h$  and  $\lambda_{air}$  are the areas of the motor components where natural convection occurs and air thermal conductivity, respectively.  $d_h$  represents the characteristic length of these motor components. The Nusselt number  $Nu_1$  is calculated by the Prandtl number  $Pr$  and the Grashof number  $Gr$ , which is proportional to the temperature difference  $\Delta T_{motor-air}$  between the motor and air. High speed and current lead to high motor temperature. Thus, the resistances  $R_{FES-C}$  and  $R_{PM-A}$  decrease with increasing speed and current.

The thermal resistances between the stator and rotor are given by the following formulas:

$$R_{stator-rotor} = \frac{1}{h_2 A_a} \quad (44)$$

$$h_2 = \frac{Nu_2 \lambda_{air}}{2l_g} \quad (45)$$

$$Nu_2 \propto \omega_r \quad (46)$$

in which  $h_2$  is the air gap convection coefficient.  $A_a$  is the air gap convection surface area and  $l_g$  is the airgap length. The Nusselt number  $Nu_2$  is the function of and proportional to rotor speed. Therefore, higher speed results in smaller stator-

to-rotor resistances. Similarly to natural convection, air gap convection is temperature-dependent, as rising air gap temperature due to rising motor temperature leads to the increase in air thermal conductivity  $\lambda_{air}$ . As a result, the resistances  $R_{PM-FES}$ ,  $R_{PM-W}$  also decrease in value with rising stator current.

The resistance  $R_{W-FES}$  is expected to be constant, because heat conduction is not affected by motor operating conditions and temperature. The dependency of  $R_{W-FES}$  in Fig. 4 on the motor speed and current can be explained by the nature of the EKF algorithm — searching for the parameters that guarantee the best fit between the temperature measurements and temperature estimations. This means even slightly different test conditions or small inaccuracies from the testing devices would lead to the variations in the identified parameters. The irregular changes in the values of  $R_{PM-FES}$  may also be the result of it. However, most of the values of  $R_{W-FES}$  remain in a range of  $[0.8 \text{ }^\circ\text{C/W}, 1 \text{ }^\circ\text{C/W}]$ .

### 3.3. Thermal Parameter Validation

It is difficult to quantify the possible errors in the identified thermal parameters. In general, a thermal network for a machine is not unique. Therefore, it is only possible to evaluate the outcome of the thermal network identification by evaluating the temperature estimation, validated by performing the open-loop tests, in which the node temperatures are calculated using the discrete-time thermal model (11)-(12), assuming the resistances are the identification results. The thermal resistances shown in Figs. 3-7 are entered into five two-dimensional (speed, current) look-up tables (2-D LUTs) in order to generate the dynamics of the thermal resistances in response to the load profile.

A simplified driving cycle where the motor speed and current change in steps, as illustrated in Fig. 8, is used to create a reference thermal transient. Fig. 9 plots the estimated temperatures together with the temperature measurements, and the estimation errors are shown in Fig. 10.

Estimated temperatures show good agreement with their corresponding measurements, which indicates a good degree of accuracy for the identified thermal resistances. However, the maximum error of approximately  $6 \text{ }^\circ\text{C}$  can be observed at low-temperature region, because the thermal resistances at each operating condition can only be identified after the thermal equilibrium is reached due to their temperature dependence. This means that the temperatures will be better estimated towards the thermal steady-state.

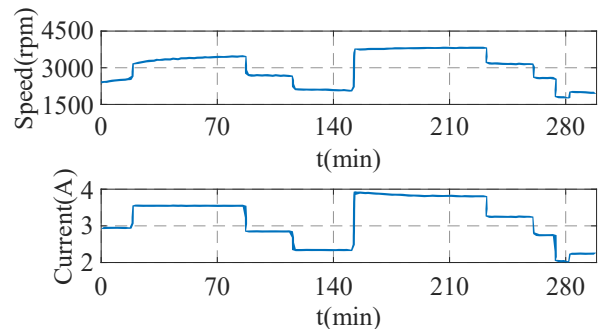


**Fig. 8.** Rotor speed and stator current profiles of the transient test

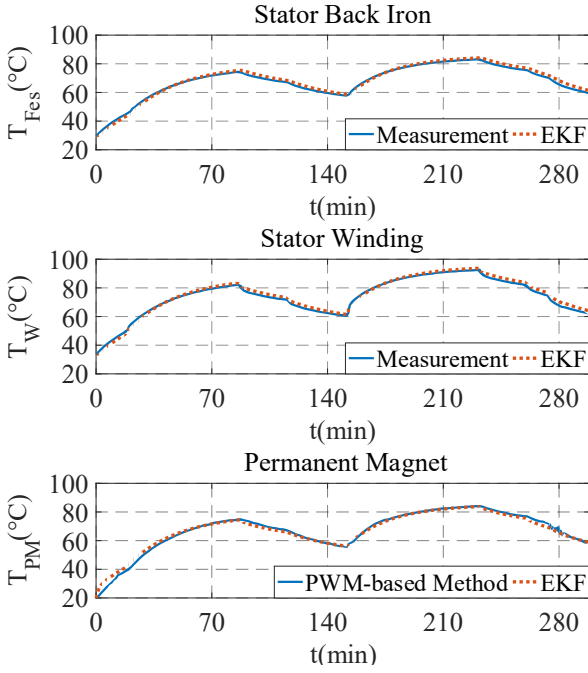


**Fig. 9.** Temperature estimations based on the transient duty cycle

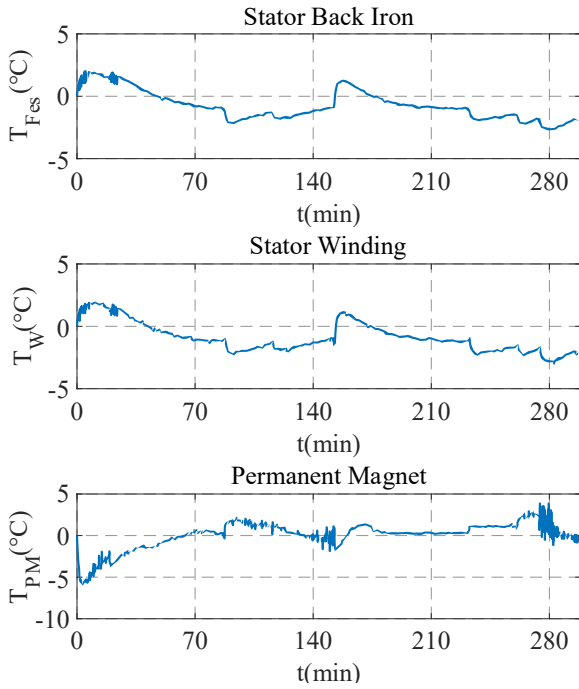


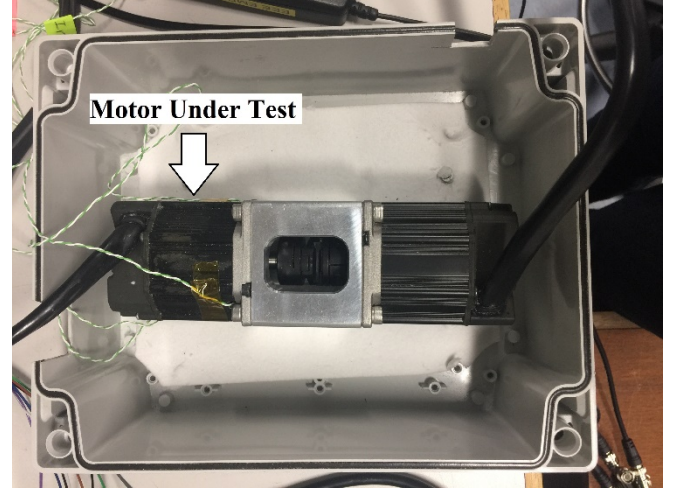
**Fig. 10.** Temperature estimation errors in Fig. 9

### 3.4. Motor Cooling Fault Detection

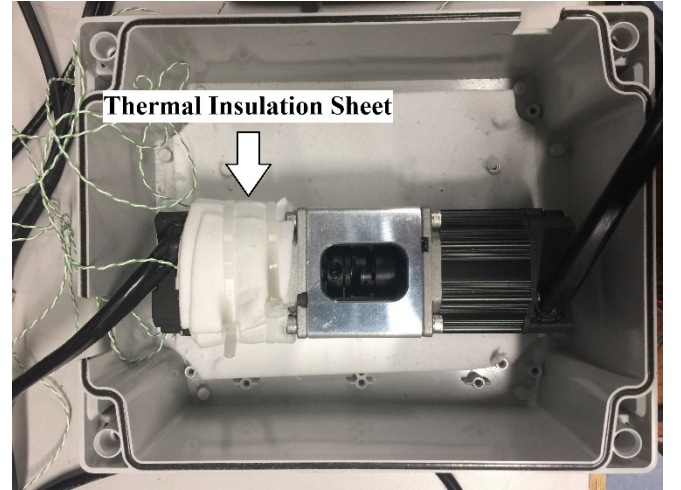
In order to validate the ability for the proposed method to detect the sudden change(s) to the cooling system in real-time, the identification procedure is performed at  $\omega_r = 3000$  rpm,  $I = 3.3$  A and two different cooling conditions. First, the rig is exposed to free air circulation to create a natural convection environment for the tested motor. After reaching the thermal steady-state, the motor is covered with

the calcium-magnesium silicate thermal insulation material which prevents heating from being transferred to the ambient. This leads to the increase in the motor temperature, as well as the thermal resistance between stator iron and cooling  $R_{Fes-c}$ . The setup is shown in Fig. 11.

The motor temperature variation as a result of this change to the cooling condition is depicted in Fig. 12(top), along with the identified thermal resistance  $R_{Fes-c}$  which as can be seen in Fig. 12(bottom), increases in response to the use of the insulation sheet. This demonstrates the possibility to employ the proposed parameter identification technique to the detection of impaired cooling conditions in PM motors [23].



*a*



*b*

**Fig. 11.** Experimental Setup

- (a) Tested motor exposed to free air
- (b) Tested motor wrapped with thermal insulation sheet

## 4. Conclusion

This paper proposes a practical and relatively simple measurement-based methodology for online identification of the thermal resistances in a three-node LPTN. The rotor temperature measurement is provided by an accurate PWM-

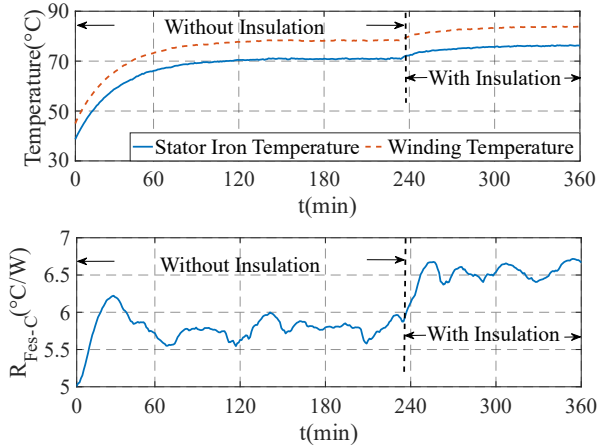


**Fig. 12.** Motor stator iron and winding temperatures (top) and the identified thermal resistance  $R_{Fes-C}$  (bottom), at two different cooling conditions

based estimation method. Therefore, the use of rotor temperature sensors which is practically difficult, can be avoided. The implementation of this method is rather simple as only the commonly measurable quantities, such as motor current, voltage and stator temperatures, are required. A typical SPMSM is employed to validate the presented method, and the result shows good precision in the identified thermal parameters. Extensive validation confirms that this method is suitable for real-time motor cooling fault/change detection. The paper demonstrates a practical online method for parameters identification with potential applications to the detection of parameters variation due to e.g. faulty conditions.

It is worth mentioning that the practical implementation of the presented method may face challenges, as standard commercial drives normally do not include voltage probes. In light of this issue, an inverter model compensating for the difference between voltage command and PWM output could be used. Also, the use of temperature sensors may increase costs. Therefore, future work would also be focusing on developing model-based estimation methods for the measurements of motor stator temperatures.

## 5. References

- [1] Karl, C., Haumer, A., and Lee, S. B.: 'A practical thermal model for the estimation of permanent magnet and stator winding temperatures', IEEE Trans. Power Electron., 2014, 29, (1), pp. 455-464.
- [2] Huber, T., Peters, W., and Bocker, J.: 'A low-order thermal model for monitoring critical temperatures in permanent magnet synchronous motors', Proc. 7<sup>th</sup> IET Int. Conf. Power Electron. Mach. Drives, Manchester, UK, Oct. 2014, pp. 1-6.
- [3] Specht, A., and Bocker, J.: 'Observer for the rotor temperature of IPMSM', Proc. 14<sup>th</sup> Int. Power Electron. Motion Control Conf., Ohrid, Macedonia, Sep. 2010, pp. T4-12 – T4-15.
- [4] Wallscheid, O., and Bocker, J.: 'Global identification of a low-order lumped-parameter thermal network for permanent magnet synchronous motors', IEEE Trans. Energy Convers., 2016, 31, (1), pp. 354-365.
- [5] Dymond, J., Ong, R., and Stranges, N.: 'Instrumentation, testing and analysis of electric machine rotor steady-state heating', Petro. Chem. Ind. Conf., IEEE Ind. Appl. Soc. 48<sup>th</sup> Annu., Toronto, Canada, Sep. 2001, pp. 297-303.
- [6] Mejuto, C., Mueller, M., Shanel, M., et al.: 'Improved synchronous machine thermal modelling', Proc. 18<sup>th</sup> Int. Conf. Electrical Mach., Vilamoura, Portugal, Sep. 2008, pp. 1-6.
- [7] Reigosa, D., Briz, F., Degner, M. W., et al.: 'Magnet temperature estimation in surface PM machines during six-step operation', IEEE Trans. Ind. Appl., 2012, 48, (6), pp. 2353-2361.
- [8] Karl, C., Haumer, A., Haigis, M., et al.: 'Comparison of a CFD analysis and a thermal equivalent circuit model of a TEFC induction machine with measurements', IEEE Trans. Energy Convers., 2009, 24, (4), pp. 809-818.
- [9] Hou, Z., and Gu, G.: 'Wireless rotor temperature measurement system based on MSP430 and nRF401', Proc. Int. Conf. Electrical Mach. Syst., Wuhan, China, Oct. 2008, pp. 858-861.
- [10] Fernandez, D., Reigosa, D., Tanimoto, T., et al.: 'Wireless permanent magnet temperature and field distribution measurement system for IPMSMs', Proc. IEEE Energy Convers. Cong. Expo., Montreal, Canada, Sep. 2015, pp. 3996-4003.
- [11] Ganchev, M., Umschaden, H., and Kapeller, H. J.: 'Rotor temperature distribution measuring system', Proc. 37<sup>th</sup> Annu. Conf. IEEE Ind. Electron. Soc., Melbourne, Australia, Nov. 2011, pp. 2006-2011.
- [12] Wilson, S. D., Stewart, P., and Taylor, B. P.: 'Methods of resistance estimation in permanent magnet synchronous motors for real-time thermal management', IEEE Trans. Energy Convers., 2010, 25, (3), pp. 698-707.
- [13] Ramakrishnan, R., Islam, R., Islam, M., et al.: 'Real time estimation of parameters for controlling and monitoring permanent magnet synchronous motors', Proc. IEEE Int. Electric Mach. Drives Conf., Miami, USA, May 2009, pp. 1194-1199.
- [14] Calin, M. D., and Helerea, E.: 'Temperature influence on magnetic characteristics of NdFeB permanent magnets', Proc. 7<sup>th</sup> Int. Symp. Adv. Topics Electrical Eng., Bucharest, Romania, May 2011, pp. 1-6.
- [15] Liu, K., Zhu, Z., and Stone, D.: 'Parameter estimation for condition monitoring of PMSM stator winding and rotor permanent magnets', IEEE Trans. Ind. Electron., 2013, 60, (12), pp. 5902-5913.
- [16] Wallscheid, O., Specht, A., and Bocker, J.: 'Observing the permanent magnet temperature of synchronous motors based on electrical fundamental wave model quantities', IEEE Trans. Ind. Electron., 2017, 64, (5), pp. 3921-3929.
- [17] Mellor, P. H., Roberts, D., and Turner, T. R.: 'Lumped parameter thermal model for electrical machines of TEFC design', IEE Proc. B Electric Power Appl., 1991, 138, (5), pp. 205-218.
- [18] Demetriades, G. D., de la Parra, H. Z., Andersson, E., et al.: 'A real-time thermal model of a permanent-magnet synchronous motor', IEEE Trans. Power Electron., 2010, 25, (2), pp. 463-474.

- [19] Wallscheid, O., and Bocker, J.: 'Design and identification of a lumped parameter thermal network for permanent magnet synchronous motors based on heat transfer theory and particle swarm optimization', Proc. 17<sup>th</sup> Eur. Conf. Power Electron. Appl., Geneva, Switzerland, Sep. 2015, pp. 1-10.
- [20] Chen, X., Wang, J., and Griffio, A.: 'A high-fidelity and computationally efficient electro-thermally coupled model for interior permanent-magnet machines in electric vehicle traction applications', IEEE Trans. Transport. Electrific., 2015, 1, (4), pp. 336-347.
- [21] Karl, C., Haumer, A., and Lee, S. B.: 'Robust thermal model for the estimation of rotor cage and stator winding temperatures of induction machines', Proc. 20<sup>th</sup> Int. Conf. Electrical Mach., Marseille, France, Sep. 2012, pp. 1810-1816.
- [22] Wallscheid, O., and Bocker, J.: 'Design and empirical identification of a lumped parameter thermal network for permanent magnet synchronous motors with physically motivated constraints', Proc. IEEE Int. Electric Mach. Drives Conf., Coeur d'Alene, USA, May 2015, pp. 1380-1386.
- [23] Zhang, P., Du, Y., Dai, J., et al.: 'Impaired-cooling-condition detection using DC-signal injection for soft-starter-connected induction motors', IEEE Trans. Ind. Electron., 2009, 56, (11), pp. 4642-4650.
- [24] Xiao, S., and Griffio, A.: 'PWM-based flux linkage and rotor temperature estimations for permanent magnet synchronous machines', IEEE Trans. Power Electron., 2020, 35, (6), pp. 6061-6069.
- [25] Xiao, S., and Griffio, A.: 'PWM-based flux linkage estimation for permanent magnet synchronous machines', Proc. 9<sup>th</sup> IET Int. Conf. Power Electron. Mach. Drives, Liverpool, UK, Apr. 2018, pp. 1-5.
- [26] Mellor, P. H., Wrobel, R., and Holliday, D.: 'A computationally efficient iron loss model for brushless AC machines that caters for rated flux and field weakened operation', Proc. IEEE Int. Electric Mach. Drives Conf., Miami, USA, May 2009, pp. 490-494.
- [27] Chen, X., Wang, J., Sen, B., et al.: 'A high-fidelity, computationally efficient model for interior permanent magnet machines considering the magnetic saturation, spatial harmonics and iron loss effect', IEEE Trans. Ind. Electron., 2015, 62, (7), pp. 4044-4055.